Available online at www.sciencedirect.com

SCIENCE DIRECT®

Tectonophysics 388 (2004) 103–117

TECTONOPHYSICS

www.elsevier.com/locate/tecto

On the nature of mantle heterogeneities and discontinuities: evidence from a very dense wide-angle shot record

Ramon Carbonell*

CSIC-Inst. Earth Sciences, Lluis Sole I Sabaris s/n, Jaume Almera, 08028 Barcelona, Spain

Received 2 July 2003; received in revised form 29 January 2004; accepted 13 June 2004

Abstract

A seismic survey with a receiver spacing of 50 m provided one of the most densely sampled wide-angle seismic reflection images of the lithosphere. This unique data set, recorded by an 18-km-long spread, reveals that at wide-angles the shallow subcrustal mantle features high amplitude reflectivity which contrasts with a lack of reflectivity at latter travel times. This change in the seismic signature is located at approximately 120–150 km depth, which correlates with the depth estimates of the lithosphere–asthenosphere boundary (LAB) of previous DSS studies. This seismic signature can be simulated by two-layer mantle model. Both layers with similar average velocities differ in their degree of heterogeneity. The shallow heterogeneous layer and the deeper and more homogeneous one correlate with the lithosphere and the asthenosphere, respectively. Studies involving surface outcrops of ultramafic massifs and mantle xenoliths infer that the upper mantle is a heterogeneous mixture of ultramafic rocks (lherzolites, harzburgites, pyroxenites, peridotites, dunites, and small amounts of eclogites). Laboratory measurements of physical properties of these mantle rocks indicate that compositional variations alone can account for the wide-angle reflectivity. A temperature increase would homogenize the mixture, decreasing the seismic reflection properties due to melting processes. It is proposed that this would take place below 120–150 km (1200 °C, the LAB).

Keywords: Wide-angle seismic reflection; Petro-physical model; Uralides; Lithosphere–asthenosphere boundary

1. Introduction

The structure and composition of the upper mantle are still unknown and are controversial issues for the Earth sciences. The mantle "stratigraphy", and mantle lithology are very difficult topics to address. The only means to obtain direct knowledge on the mantle composition are the very limited surface exposures of upper mantle units and the petrological study of xenoliths. Recent advances in geothermobarometry and trace element analysis allow the determination of equilibration temperatures of individual grains of a concentrate. These data can be placed in a temperature depth context and provide a way to map mantle

* Tel.: +34 9340 95410; fax: +34 9341 10012.
E-mail address: rcarbo@ija.csic.es.

0040-1951/$ - see front matter © 2004 Elsevier B.V. All rights reserved.
doi:10.1016/j.tecto.2004.07.025

"stratigraphy" in terms of rock types and fluid related processes (Griffin et al., 1996). Geochemical comparison of mid-ocean ridge basalts and ocean island basalts has also provided mantle models. However, the chemical observations can be explained by a variety of models. Petrological models for the mantle are also controversial. Some models assume a mantle divided into a depleted upper mantle and an undepleted lower mantle, responsible for the mid-ocean ridge and ocean island basalts, respectively. Two alternative models have been proposed which also explain the chemical observations: a layered mantle model (Anderson, 1990) and the strongly heterogeneous plum-pudding mantle model (Morgan, 1997; Morgan and Morgan, 1999).

Seismic surveys provide direct measurements of the physical properties (P- and S-seismic velocities) which constitute another link to the mantle structure. Controversy on the velocity structure of the upper mantle date from the early 1950s. Two of the earliest and best-known models of seismic velocities of the Earth, one by Jeffreys and a second by Gutemberg, differ at depth. Gutemberg's model requires a low velocity zone at 100–150 km depth to explain the 20° discontinuity, while Jeffreys' model does not (Anderson, 1990). Interpretations of the first long-range explosion seismic experiments suggested a heterogeneous velocity structure for the upper mantle (Willmore, 1949). Since then, the existence, depth and nature of major mantle discontinuities has been discussed by seismologists intensively; for example the 400 km (Jeffreys, 1936), and the 220 km discontinuities (Lehmann, 1964).

Since the early 1980s, the structure of the upper mantle has been one of the main topics of research in Earth Science (Pavlenkova, 1996; Thybo and Perchuc, 1997; Perchuc and Thybo, 1996; Nolet, 1994; for example). Expensive active source deep seismic reflection/refraction experiments have been devoted to study the upper mantle, for example GNOME, Early Rise (Iyer and Hitchcock, 1989), FENOLORA (Guggisberg and Berthelesen, 1997), the Peaceful Nuclear Explosions (PNE) (Yegorkin et al., 1987) and most recently the Deep Probe (Henstock et al., 1998). New two-dimensional interpretations of these seismic data sets show strong lateral variations of the velocity structure within the upper mantle commonly interpreted as alternating high and low velocity layers (Mechie et al., 1993; Ryberg et al., 1995, 2000; Ryberg and Wenzel, 1999; Tittgemeyer et al., 1996, 1999; Morozov et al., 1998; Morozov and Smithson, 2002; Nielsen et al., 2003a,b). These studies and the interpretation of passive teleseismic studies, which are characterized by low resolving power, reveal heterogeneities at all scales within the upper few kilometers of the mantle (Nolet, 1994). Upper mantle heterogeneities have been considered as responsible for the high frequency teleseismic Pn event recorded in the far offset wide-angle PNE shot records (Ryberg et al., 1995, 2000; Ryberg and Wenzel, 1999; Tittgemeyer et al., 1996; Morozov et al., 1998; Nielsen et al., 2003a,b). Pn is then interpreted as a result of a whispering gallery, multiply reflected and refracted wave within the upper mantle (Menke and Richards, 1983). A number of recent studies (Calvert et al., 1995; Pavlenkova, 1996; Perchuc and Thybo, 1996; Warner et al., 1996; Thybo and Perchuc, 1997; Carbonell et al., 2002; Nielsen et al., 2003a,b; among others) associate the complex velocity structure with stratified lithospheric mantle and propose a number of possible mechanisms for its development, including partial melting, phase transition, compositional changes, trapped fluids, thermal boundary and tectonic process related alterations.

The new technical improvements in seismic recording has allowed a large number of recent deep seismic multichannel reflection studies from different parts of the world and from different geologic settings to observe near vertical and wide-angle reflections from the continental mantle (Calvert et al., 1995; Warner et al., 1996; Steer et al., 1998; Cook et al., 1999; Carbonell et al., 2000, 2002). Although, the geotectonic origin and significance of these events can be uncertain, their location in the vicinity of major orogenic features suggests that such anomalous reflective regions were developed as a result of the direct involvement of the subcrustal lithosphere in the tectonic processes affecting the overlying crust. Because of the demonstrated coupling between the crust and lithospheric mantle (Zhao and McCulloch, 1993; Chen et al., 1994), information on the internal structure, nature and composition of the upper mantle is an asset to understanding the processes that affect it, and which play an active role on the mechanisms and timing of large-scale tectonic events that influence the crust.

The aim of this study is to present one of the highest resolution wide-angle images of the upper mantle ever obtained and the analysis of the seismic signature in the

light of the existing geochemical knowledge from xenoliths and limited surface exposures. The wide-angle data discussed in this paper are unique in several aspects. Wide-angle data are often acquired with average trace spacing larger that 250 m. The shot gather presented here features a trace spacing (50 m) which is not common in on-land seismic wide-angle data acquisition. This wide-angle image acquired in the Urals features an unusually high lateral resolution. Additionally, the midpoint between the source and receiver locations lies in the center of the Urals mountain range, sampling the root zone beneath the core of the orogen. The upper mantle structure (beneath the crustal root zone) is the result of mountain building orogenic processes. Although, densely recorded onshore–offshore wide-angle data were acquired during the BABEL and the MONA LISA in the Baltic Sea and the North Sea, respectively, these data sets do not address mountain building orogenic processes. Thus, the seismic image is probably unique in the sense that it is an imaging process, which is not common in seismic surveys of other orogenic zones like the Appalachians or the Caledonides.

2. The wide-angle seismic reflection image of the lithosphere

The high-resolution deep seismic wide-angle data set analyzed in this study was acquired during the URSEIS'95 (Berzin et al., 1996) multiseismic experiment. This seismic data acquisition experiment which was acquired across the Southern Urals (Fig. 1), consisted of three main components: (1) a normal incidence Vibroseis source component; (2) a normal incidence explosive source component and, (3) a wide-angle component. Description of the objectives, acquisition parameters, processing and different interpretations have been published elsewhere (Echtler et al., 1996; Carbonell et al., 2000, 2002). Nevertheless, the wide-angle densely recorded shot gather has never been displayed or discussed. The three experiments started at approximately the same time. The normal incidence data was acquired using a 360 channel input/output seismograph with a 18-km-long cable with stations distributed every 50 m. For the wide-angle experiment, 1 to 3 ton explosion shots were used. The acoustic energy released by these shots was recorded by 50 three component digital seismographs (LENNARTZ and REFTEKS). Because the three experiments started at approximately the same time, the wide-angle shot point 1 was also recorded by the 360 channel input/output seismograph (Fig. 1). The 18-km-long recording spread was located at an offset distance of 310–328 km. The image is one of the highest resolution wide-angle images obtained of the lithosphere since today because it images up to approximately 200-km depth (Fig. 2) with a surface (horizontal) sampling interval of 50 m. Qualitatively, the shot gather displays two characteristic horizontal bands. A highly reflective band from −3.5 to 4.0 s reduced travel time (6 km/s) and a more transparent one from 4.0 to 10 s reduced travel time (Fig. 2).

Conventional ray tracing modeling suggests that all of the most prominent crustal arrivals at this offset range should be recorded within the time window between −3.5 and −2 s reduced travel time (Fig. 3). The velocity model derived from the interpretation of the refraction data (Carbonell et al., 2000) was used for the ray tracing. This time window includes the first arrival and the PmP as the most prominent phases. These phases are laterally continuous and characterized by high amplitudes for the 18-km profile covered by the shot record. Below the crustal reflectivity, the shot gather displays a densely laminated fabric of relatively horizontal events which are, on average from 4 to 6 km long. The band between 3 to 9 s is clearly less reflective and, more transparent. Nevertheless, a few linear, and relatively short events can be distinguished for example at 314 km offset at 4, 7 and 8 s, and at 324 at 4 and 8 s. The events within this band are less laterally continuous being less than 2 km long.

With the aim of characterizing the reflectivity above and below 3 s, the amplitude decay curve and the frequency content of two 3 s long time windows, one between −3.0 and 0.0 s and a second one between 5.0 and 8.0 s, were analyzed (Fig. 4). The amplitude decay curve reveals that the most prominent events in the reflective and in the transparent bands feature amplitude maxima of similar magnitudes. For example, the events at approximately −2, 0, 1, 2, 4, and 7 s (Fig. 4). The amplitude decay curve also displays the behavior of the average amplitude which increases from 500 amplitude units (AU) to over 2000 AU at −2 s, then it stays, approximately, constant (over 2000

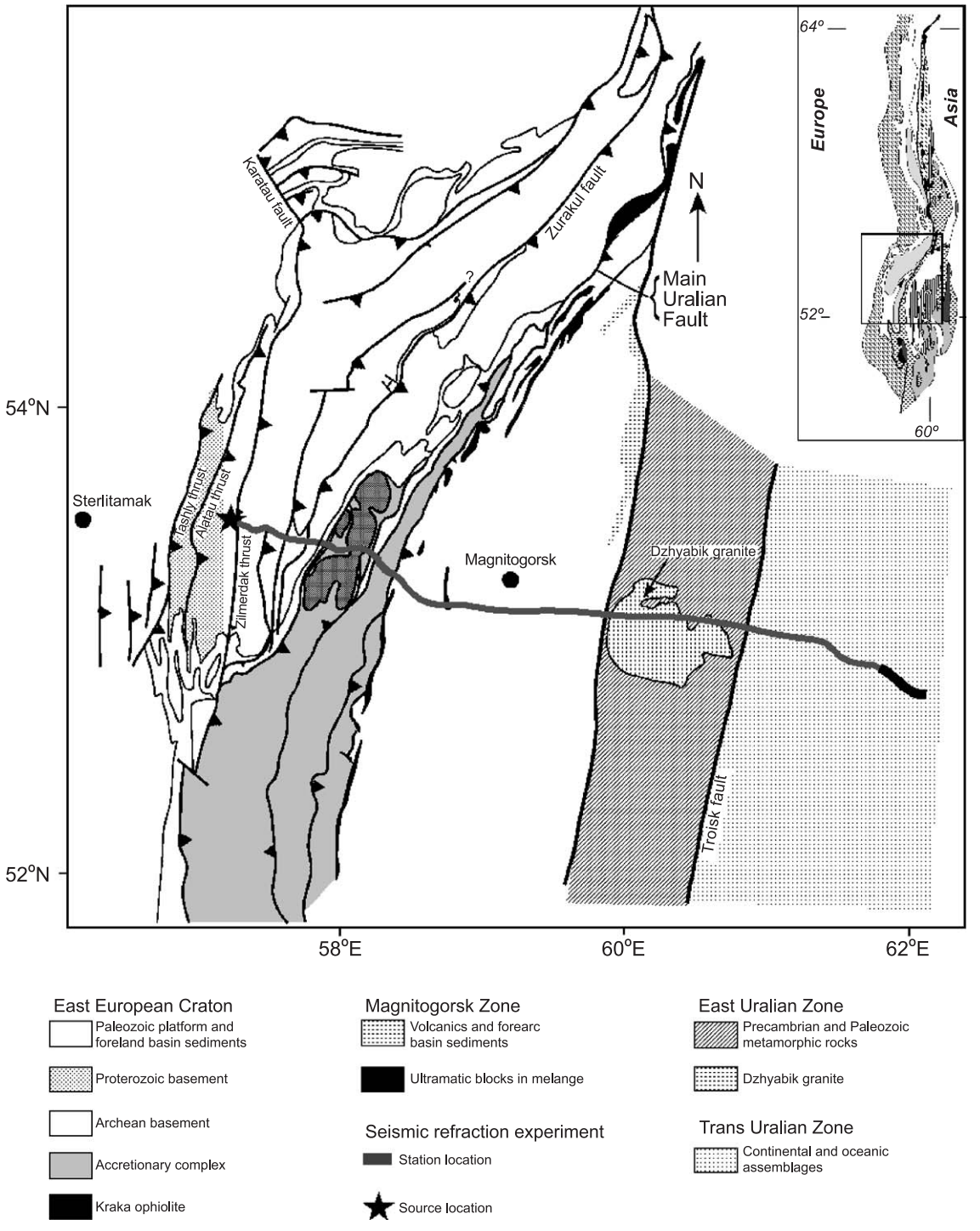
64°
Europe
Asia
52°
60°
Karatau fault
Zurakul fault
N
Main
Uralian
Fault
?
54°N
Sterlitamak
Iashly thrust
Alatau thrust
Zilmerdak thrust
Magnitogorsk
Dzhyabik granite
Troisk fault
52°N
58°E
60°E
62°E
East European Craton
Paleozoic platform and foreland basin sediments
Proterozoic basement
Archean basement
Accretionary complex
Kraka ophiolite
Magnitogorsk Zone
Volcanics and forearc basin sediments
Ultramatic blocks in melange
Seismic refraction experiment
Station location
Source location
East Uralian Zone
Precambrian and Paleozoic metamorphic rocks
Dzhyabik granite
Trans Uralian Zone
Continental and oceanic assemblages

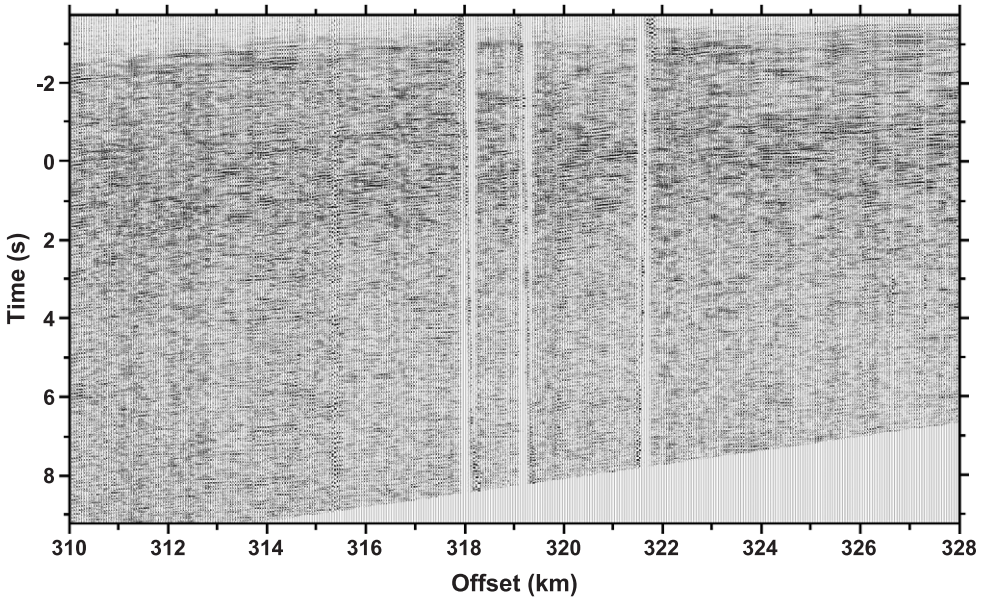

Fig. 2. Spatially dense high-resolution seismic shot record acquired in the southern Urals by the seismic reflection 360 channel input/output seismograph. The source used was the 3000-kg shot fired from shot point 1 for the seismic refraction/wide-angle experiment. The offset range was approximately 310–328 km. The data has been reduced by 6 km/s velocity in order to compare with Fig. 3. The traces have been normalized by the rms amplitude of the noise. The rms amplitude of the noise has been estimated using a 1-s-long time window before the first arrival.

AU) until 2 s and then decrease to about 1000 units at 9 s. Notice that the shot gather features a 5-s window where the average amplitude is relatively high. The amplitude decay curve (Fig. 4) is consistent with a coda overlain by some fairly deep high amplitude reflections.

The frequency content for both time windows is displayed in Fig. 4. The data were recorded using geophones with a 10-Hz natural frequency. Therefore, the signal has a frequency content between 10 and 40 Hz in both windows. The window between −3.0 and 0.0 s displays high frequency content at 12–17 Hz and at 20–26 Hz. The 5.0–8.0 s window features relatively high amplitude content between 12 and 15 Hz frequencies. Both spectra are similar below 20 Hz. The frequency band above 20 Hz has been attenuated at the later window (Fig. 4).

3. Physical properties of mantle rocks

The lithological composition of the upper mantle can be inferred by studying the tectonically emplaced ultramafic massifs in orogenic belts and samples of ultramafic material which has come to the surface such as mantle xenoliths (Downes, 1997). These studies reveal that layered sequences of eclogites with different chemical compositions, and very heterogeneous layers featuring a mixture of lherzolites, harzburgites, pyroxenites, peridotites and dunites are common in the upper mantle. The very limited surface outcrops of lower crust to upper mantle sequences such as the Cabo Ortegal area (Northwestern Iberia Peninsula), Ivrea (Northern Italy), the exposures of mantle rocks such as the Ronda (Southern Iberia Peninsula) and Beni-Bousera (Northern Morocco),

Fig. 1. Location of the URSEIS'95 deep seismic experiment. Geologic sketch map indicating the major geologic units and tectonic structures of the southern Urals. Top inset map shows the location of the study area in the southern Urals. The URSEIS'95 normal incidence seismic reflection transects indicated by a gray line. The location of the wide-angle shot 1, which was recorded by the input/output seismograph and that discussed in the text, is indicated by a star. The location of the seismic reflection recording cable is denoted by a bold black line; 50 m was the station spacing of the sensors (standard seismic exploration geophones, with a 10-Hz natural frequency).

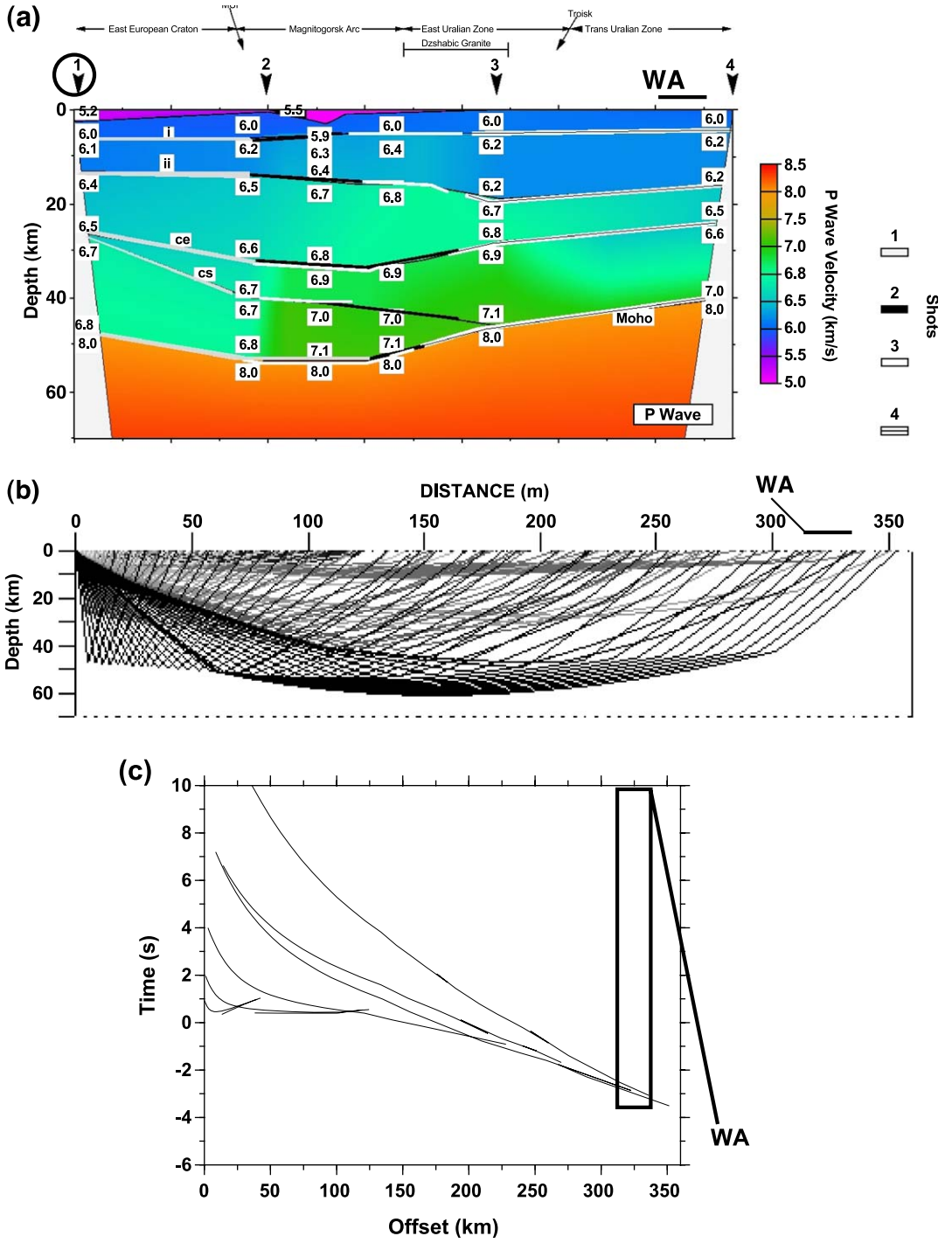

Fig. 3. (a) Velocity model derived by travel time interpretation of the refraction data (Carbonell et al., 2000). Shot 1 corresponds to the source point of the densely sampled wide-angle image. (b) Synthetic ray paths for shot 1 (reduced travel time (rtt)) using 6 km/s. The location of the recording cable is indicated by a bold line labeled WA. (c) Synthetic travel times for shot 1 indicating the subset recorded by the densely spaced wide-angle image. Notice that all the crustal arrivals are recorded within the −2 to −4 s rtt window for offsets greater than 300 km. Please refer to the web version of the paper to view this figure in colour.

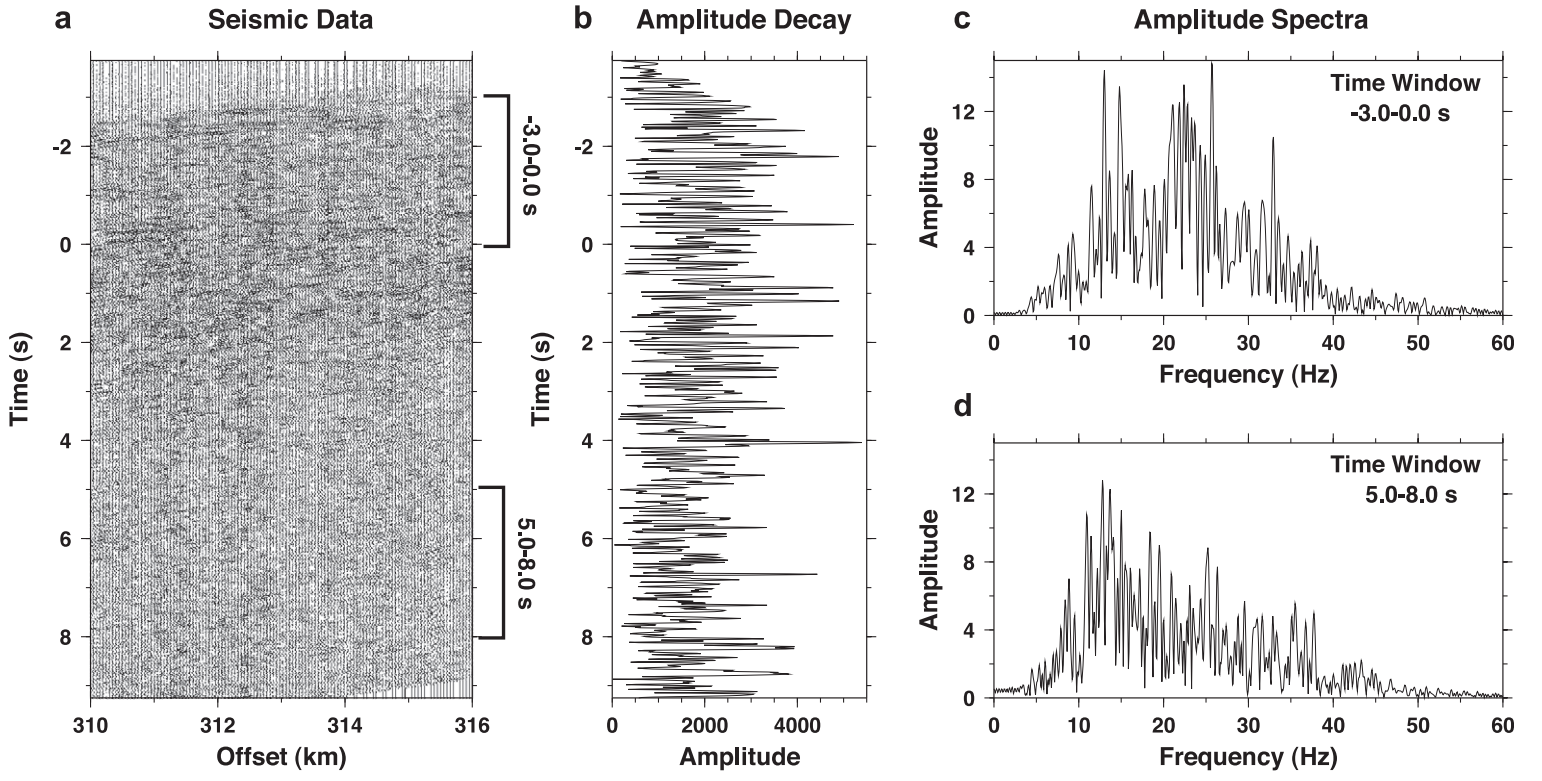

Fig. 4. Amplitude and spectral character of the high-resolution wide-angle seismic shot gather. (a) Detail image of the seismic data. The traces displayed have been used to obtain the amplitude decay curve. The time windows marked between −3.0–0.0 and 5.0–8.0 s reduced travel time correspond to the time windows used to obtain the amplitude spectra. (b) Amplitude decay curve as a function of time. This curve was obtained by adding the seismic traces displayed in (a) after they had been corrected for spherical divergence. The amplitude decay is the envelope of the trace resulting from staking the traces displayed in (a). Note that the amplitudes between −3.0 and 0.0 s, which corresponds to the crust and upper mantle, are of similar magnitude as the amplitudes in the deeper window which probably corresponds to backscattered energy (far offset diffractions) caused by heterogeneities within the asthenosphere. The decrease in the reflectivity at approximately 3.0 s most probably corresponds to the lithosphere–asthenosphere boundary (see text for explanation). (c) Average amplitude spectrum displaying the frequency content of the seismic data within the time window between −3.0 and 0.0 s, (d) Average amplitude spectrum displaying the frequency content of the seismic data within the window 5.0–8.0 s. Note that similar frequencies are observed in both diagrams.

and the tectonically emplaced ultramafic massifs of the Pyrenees and Alps, all reveal structural complexities such as pyroxenite layering, harzburgite bands and several generations of crosscutting mafic and ultramafic dykes. Commonly these ultramafic units display laminated or banded structures composed of interlayering of lherzolite, harzburgite, pyroxenite, peridotites, dunites, among other types of dense rocks and minerals. Most of the ultramafics contain high amounts of olivine and garnet. Ultramafic massifs can have pyroxenite bands which can be well defined or diffused and with a thickness that can range from a few millimeters to a few meters. Additionally, harzburgite can be found in bands up to 20 m thick and parallel to the pyroxenite layering. Surface outcrops of mantle peridotites are typically found to be a mixture of basalt–pyroxenite veins embedded within a harzburgite–lherzolite matrix. For example, the Ronda and Beni-Bousera ultramafic massifs contain pyroxenite veins, with 10-m to 10-km length scales. These rock types are also common in xenolith suites. The structural and petrological complexities in the field observations, the tectonic fabrics and the variability in the laboratory measurements of physical properties reveal the existence of heterogeneities at all scales. For example in xenoliths, amphibolite veins cut peridotite, and in massifs meter-scale layers of pyroxenite appear cutting a peridotite matrix. As the kilometer-scale heterogeneities can be identified in the differences in petrological composition between adjacent massifs, this characteristic feature should be detectable by geophysical methods (Downes, 1997) in particular by seismic techniques.

A physical properties database (density, seismic velocities, seismic attenuation) was build from published studies of laboratory measurements on rock samples from different areas and from different tectonic environments and on mantle xenoliths (Carmichael, 1989; Long and Christensen, 2000; Gao et al., 2000; among others). The database was developed to evaluate if the differences mapped at outcrop scale can be detected by seismic methods (Fig. 5). The density and P-wave velocity values for each rock sample are plotted in Fig. 5. These ultramafic rocks feature high densities (3.0–4.4 kg/cm^3) and relatively high P-wave velocity values (within the range 6.70–8.75 km/s). Both range of values is broad enough so that the juxtaposition of different rock types or, even the juxtaposition of different samples of the same rock type can result in relatively high reflection coefficients. Thus the variability of the seismic velocities and densities within these rock types can result in significant reflection coefficients (Fig. 5).

For each specific rock type, a random stratigraphic column, "stochastic single rock type model" was build by randomly choosing, from the physical properties database, samples of that particular rock type and juxtaposing them. Then the reflection coefficients for the stratigraphic column were calculated and a histogram of the population of the reflection coefficients as a function of frequency was plotted (Fig. 5). Fig. 5 reveals that stratigraphic columns characterized by the superposition of different samples of a single rock type can produce relatively high reflection coefficients. For example, a stratigraphic column composed by peridotite layering can have reflection coefficients greater than ± 0.1 while reflection coefficients of ± 0.1 are not possible or have very low frequency for single rock type stratigraphic columns of dunite, of eclogite, or of harzburgite. The variety in the physical properties of pyroxenite samples can also result in high reflection coefficients. Fig. 5 indicates that the stochastic stratigraphic columns of peridotite and pyroxenite can cause reflectivity, while dunite, harzburgite and eclogite are less capable of causing seismic reflections.

These rock types are all found forming complex structural relations in the limited surface exposures of ultramafic massifs. Rock samples from the same area can have small differences in percentages of the constituent minerals, which causes important differences in the physical properties. For example, differ-

Fig. 5. Stochastic estimation of the reflection coefficients for the lithosphere from physical properties of mantle rocks. (a) Database of the physical properties (density and seismic velocities of P (compressional) waves) of rock samples characteristic of the upper mantle. (Carmichael, 1989; Kern et al., 1999; Gao et al., 2000). A relatively large number (5000) of layered models were generated by randomly selecting velocity–density pairs from the database. (b–f) Distributions of the reflection coefficients for layered models consisting of single rock types, eclogite, peridotite, dunite, harzburgite and, pyroxenite, respectively. (g) Distribution of the reflection coefficients for layered mantle models consisting of mixtures of the rock types previously specified.

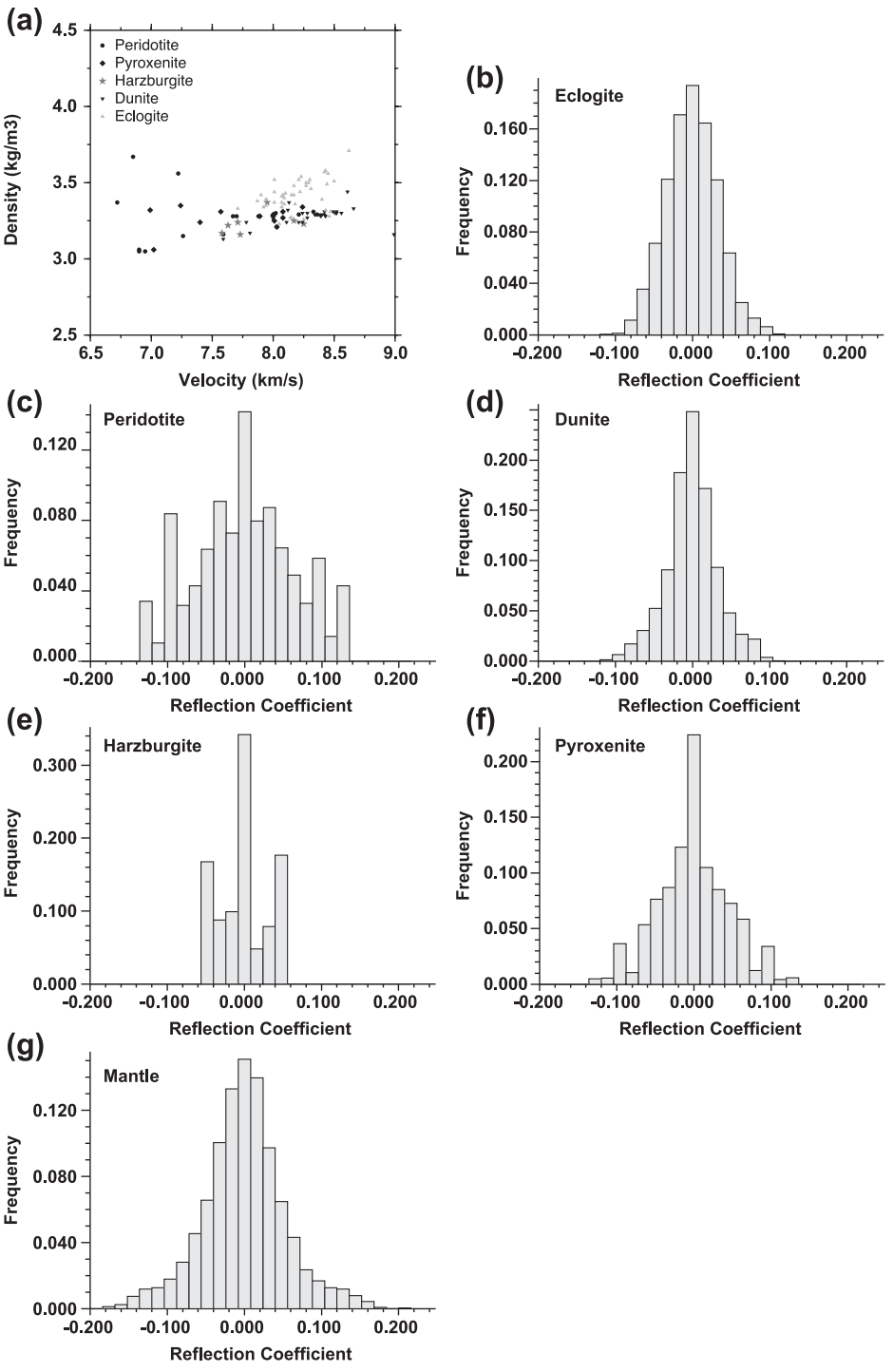
(a)
Peridotite
Pyroxenite
Harzburgite
Dunite
Eclogite
Density (kg/m3)
Velocity (km/s)
(b)
Eclogite
Frequency
Reflection Coefficient
(c)
Peridotite
Frequency
Reflection Coefficient
(d)
Dunite
Frequency
Reflection Coefficient
(e)
Harzburgite
Frequency
Reflection Coefficient
(f)
Pyroxenite
Frequency
Reflection Coefficient
(g)
Mantle
Frequency
Reflection Coefficient

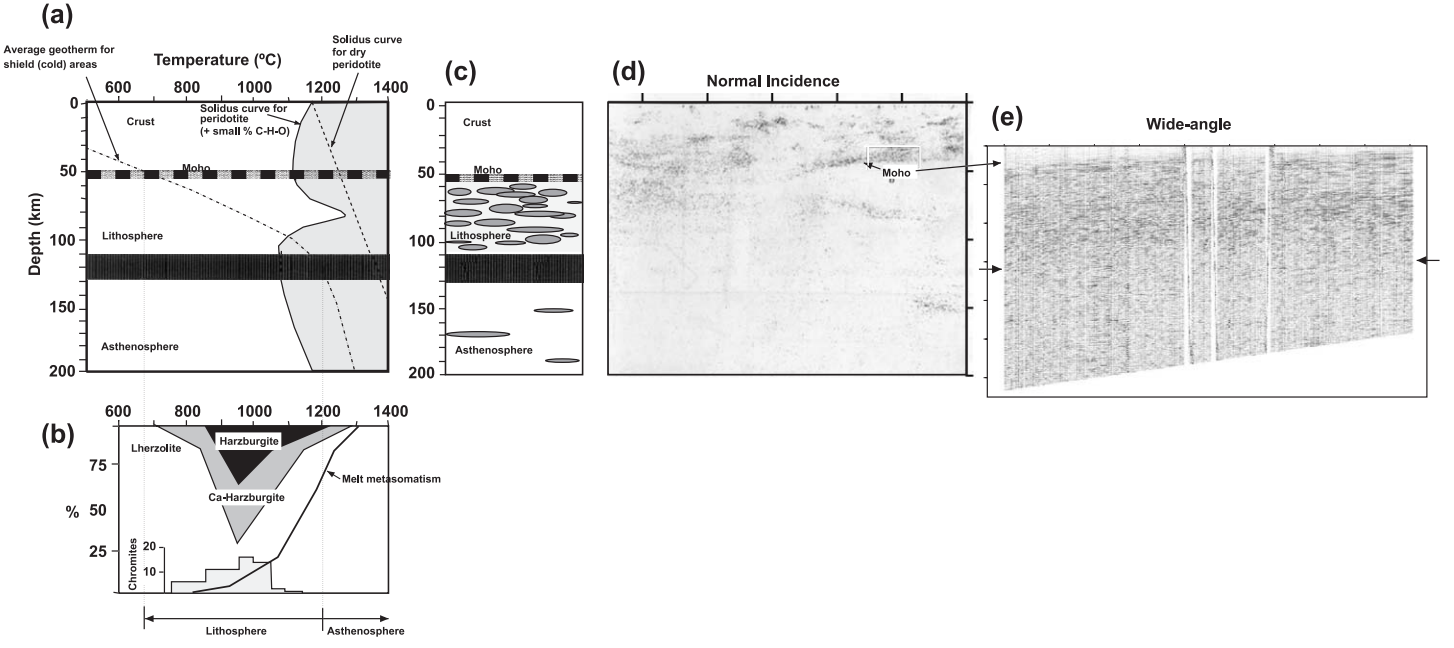

Fig. 6. Interpretative model of the lithosphere beneath the Urals. (a) Temperature depth diagram on which the solidus curve for peridotite with small percentage of CO_2 and H_2O, the solidus curves for dry peridotite, and the average geotherm for shield (relatively cold) areas (approximately 60 mW/m^2) have been drawn. The Moho, the lithosphere, and the asthenosphere are also indicated. (b) Geochemical results of the analysis of mantle xenoliths from Griffin et al. (1996), illustrating the thermal-compositional profile of the mantle, the modal composition of the analyzed xenoliths showing the percentage of harzburgite and lherzolite and the change as a function of their depth origin. It also displays the variation of chromites with temperature. The melt metasomatism curve illustrates the changes in the processes in the upper mantle indicating that the lithosphere is mostly depleted and the asthenosphere melt metasomatism processes are dominant (Griffin et al., 1996). (c) Simplified cartoon of the subcrustal heterogeneous mantle beneath the southern Urals, which would explain the seismic observations. The heterogeneities are of compositional nature. The lithosphere–asthenosphere boundary denotes a change in the temperature gradient at 110–130 km depth. Beneath it, the melt phase dominates; therefore, less heterogeneities are expected. (d) The explosive normal incidence seismic reflection image (Steer et al., 1998). (e) The densely space (50 m) wide-angle seismic record section.

ent P-wave velocities and densities for harzburgitic xenoliths from South Africa (velocities of 7.7 and 7.1 km/s and densities of 3.168 and 3.049 kg/m^3) have been reported (Long and Christensen, 2000). Additionally, tectonic fabrics (shear zones, foliation) affect the physical property measurements introducing anisotropy (Levander and Holliger, 1992; Long and Christensen, 2000). The database of the physical properties of mantle rocks is not complete, and the amount of each rock type present in the mantle is unknown; however, because of the factors which influence the physical properties it seems reasonable to use this database to generate a stochastic mantle model by randomly choosing rock samples from the entire database of physical property measurements (Fig. 5). The stochastic stratigraphic column and the histogram plot Fig. 5) illustrate that approximately 30% of the reflection coefficient population is larger than ± 0.05, indicating that compositional variations alone, within the mantle, can provide reflection coefficients high enough to cause relatively high amplitude reflections. This reflectivity can be further emphasized due to the tectonics of the area, which can generate tectonic fabrics, foliation, and sheared zones that cause anisotropy, resulting in highly reflective structures.

4. Geological and geochemical constraints on the composition of the upper mantle

A heterogeneous upper mantle is supported partly by surface exposures of ultramafic massifs and partly by the geochemical analysis of mantle xenoliths. Griffin and Ryan (1995) and Ryan et al. (1996) use geothermobarometric measurements of xenolith to provide evidence for upper mantle layering in terms of rock types. They also estimate variation in the chemical compositions of mantle xenoliths and attribute them to the depth of generation. For example, the chromite content in garnets changes within the temperature range 700–1100 °C, their experimental work and laboratory measurements indicates an initial increase of Cr_2O_3 content with depth and a subsequent decrease (Fig. 6). They also determined that depleted garnets with relatively low contents of Zr, Y and TiO_2 indicate an increase of the melt-related metasomatism above the 1200 °C. High T xenoliths show magma-related heating, recrystallization, thermal resetting of fine-grained assemblages and recrystallization (Boyd, 1984). The existence of inclusions of garnet and pyroxene grains within large olivine crystals constitutes evidence for recrystallization processes. The predominance of these melt-related signatures is regarded as reflecting a rapidly increasing influence of asthenosphere-derived material. Based on this chemical evidence, the base of the lithosphere can be located at the 1200 °C geotherm (Griffin et al., 1996). The laboratory observations reveal that the lithosphere–asthenosphere transition features large temperature gradients, which can be horizontal and vertical. The large database of xenolith suites occurring in kimberlite fields indicates that lherzolites are dominant at shallow depths (up to 900 °C), harzburgites become more abundant with increasing depths (within the temperature range of 900–1500 °C) to a maximum of 150–190 km. At greater depths, lherzolites become more abundant again (at T larger than 1100 °C) and many of these deeper lherzolites are depleted (Griffin et al., 1996). At depths larger than 220 km, nearly all reported xenolith data reveal that xenoliths are highly metasomatized and correspond to the sheared xenolith population (Griffin et al., 1996).

5. Discussion and implications

The small trace spacing (50 m) used for the acquisition of the wide-angle seismic reflection data (Fig. 2) results in an image of the crust and upper mantle characterized by an unusually high lateral resolution. Furthermore, as the reflection midpoint is located beneath the core of the Urals orogen, the seismic data images the root of a Paleozoic collision orogen. Although this wide-angle image is very limited in extent, the previous features make it unique, because it images, with an unusual resolution, upper mantle structures which are not common in seismic surveys of other orogenic zones.

The spatially dense recording of the wide-angle shot point 1 reveals that the subcrustal mantle is strongly reflective (Fig. 2). The amplitude decay curve indicates that the average amplitude within -2 to 3 s reduced travel time stays approximately constant at a little over 2000 units. The seismic signal identified after the PmP arrival in the refraction

recording of shot point 1 at 310 km offset only last for 1 to 1.5 s (Carbonell et al., 2000). This suggests that the relatively high average amplitudes within the 5-s-long window are probably not a result of reverberations within the crust. The events imaged by the wide-angle shot gather most probably correspond to far offset diffractions (backscattered energy) caused by local heterogeneities immediately beneath the core of the orogenic belt. The thickness of this proposed heterogeneous subcrustal mantle is at a first estimate from 50 to 150 km. Note that the crustal thickness beneath the central part of the orogen (which roughly corresponds to the midpoint between the source and the receiver position) is of 53±3 km (Carbonell et al., 2000).

Below 3 s (reduced travel time), the reflection character changes and the reflectivity decreases (Fig. 2). Nevertheless, a few high amplitude events can be identified. The amplitude decay looks like a coda overlain by some fairly deep relatively high amplitude reflections. The amplitude of the deepest events is of the same order of magnitude as for the earlier reflections (Fig. 4).

The frequency content (Fig. 4) of the two different time windows reveal an attenuation of frequencies above 20 Hz for the 5–8 s time window. The amplitude spectra favor relatively high values of Q that preserve frequencies below 20 Hz. In the 3–9 s time window, the events are probably far offset diffractions, or constructive interference of far offset diffractions. The small amplitude differences between the crustal and these mantle events displayed by the amplitude decay curve (Fig. 4) support this interpretation. The normal incidence data acquired during the URSEIS'95 also recorded high amplitude deep events, such as the Nikolaevka, and Alexandrovka reflection sequences (Steer et al., 1998) (Fig. 6).

Therefore, this image suggests that the subcrustal mantle beneath the southern Urals is strongly heterogeneous from 50 to 120–150 km. At this depth, the reflectivity decreases suggesting a change in the degree of heterogeneity. Beneath 150 km, the amount and size of the heterogeneities decreases and the mantle appears more homogeneous (Fig. 6). The nature of the heterogeneities is very difficult to assess; however, the xenolith studies and the limited exposure of upper mantle sequences provide key additional constraints.

The combination of the normal incidence seismic data and the high-resolution wide-angle image provide complementary information (Fig. 6). The crustal architecture is determined from the normal incidence data imaging the Moho discontinuity. Beneath the Moho, the high-resolution wide-angle data provide evidence for strongly heterogeneous subcrustal mantle down to approximately 120-km depth. At this depth, the reflectivity decreases abruptly. Within 50 to 150 km depth is where evidence from geochemistry measurements indicates that the mantle is the most heterogeneous, with the coexistence of lherzolite and harzburgite mineralogies and a variation in the amount of chromites. At approximately 120-km depth, the predicted temperature is estimated to be of 1200 °C, which is a critical temperature for the location of the lithosphere–asthenosphere boundary. The increase in temperature provides a mechanism for increasing melting processes with the result of homogenizing the media (asthenosphere). However, heterogeneities, or boudins, with slightly different physical properties mostly due to composition can have different melting temperatures and therefore a few local heterogeneities may exist which can cause reflections in seismic data. This model is probably not a general one. Nevertheless, it probably fits Paleozoic mountain roots as the Urals. The collision process has probably accentuated the heterogeneous nature of the subcrustal mantle beneath the core of the mountain chain.

A prominent mantle discontinuity is the lithosphere–asthenosphere boundary which is identified by a sharp decrease in V_p from 8.5 to 8.1 km/s approximately (Pavlenkova, 1996). The interpretation of long-range seismic data from the PNE experiments indicates that this decrease in V_p is located between 120- and 220-km depth depending on the tectonic environment. The low velocity upper mantle layer beneath the Craton and Kimberlite seismic profiles is located, approximately, at 100-and 120-km depth (Pavlenkova, 1996), and has been interpreted as a rheologically weak layer (Griffin et al., 1996). A reflective upper mantle up to 125-km depth and deepening to the south to 150 km has also been identified across the Trans Hudson Orogen (Hajnal et al., 1997). Beneath south Hungary, deep normal incidence seismic reflection images suggest that the lithosphere–asthenosphere boundary (LAB) is anom-

alously shallow (Posgay et al., 1990). A sharp decrease in shear wave velocity also indicates the location of the LAB in South Africa, where Priestley (1999) identifies significantly low shear wave velocity values between 120 and 150 km. Complex velocity–depth functions in other areas reveal velocity decreases within the 100–220 km depth interval (Gaherty and Jordan, 1995; Perchuc and Thybo, 1996; Thybo and Perchuc, 1997; Priestley, 1999). Low velocities would indeed decrease the reflectivity at wide angles. Unfortunately, the URSEIS'95 experiment does not cover the required offsets to resolve the velocities at these depths. Nevertheless, the relatively sharp change in the reflectivity pattern of the high-resolution wide-angle shot gather is indicative of a decrease in the degree of heterogeneities, suggesting a more homogeneous mantle beneath, approximately 110–140 km depth. The heterogeneous zone is interpreted as lithospheric mantle while the more homogeneous zone could be associated to the asthenosphere.

The LAB is a relatively thick transition zone that probably includes the 1200 °C isotherm. This proposed model (Fig. 6) for the subcrustal mantle is also consistent with seismic synthetic modeling studies of the high frequency Pn phase observed in Quartz and other PNE shot records (Ryberg et al., 1995, 2000; Ryberg and Wenzel, 1999; Tittgemeyer et al., 1996, 1999; Morozov et al., 1998; Morozov and Smithson, 2002; Nielsen et al., 2003a,b). In these studies, the Pn phase is a result of the seismic energy traveling within an upper mantle heterogeneous layer (lithosphere) at a depth of 50 to 180 km, approximately. Geochemical studies suggest that this heterogeneous layer is probably composed by a mixture of eclogitized rock at Moho depth underlain by lherzolites, harzburgite, pyroxenites and peridotite (Fig. 6). As depth increases melt metasomatism due to an increase in temperature homogenizes the mixture as indicated by the intersection of the proposed geotherm and the solidus curve (Fig. 6). Only lenses of material with a higher melting point survive the melting. These are the boudins that are probably responsible for the deepest reflectivity. Furthermore, the midpoint of the high-resolution wide-angle reflection image lies approximately beneath the core of the Urals orogenic belt, and the contrast between the proposed heterogeneous lithosphere and a more homogeneous asthenosphere is probably emphasized by the collision tectonics. Probably beneath the root the mantle consist of an amalgamation of boudins with crustal affinity and slices of heterogeneous mantle material with different nature. Surface outcrops, and geochemical data from xenoliths support a boudinage structure including a mixture of ultramafic rocks, such as: eclogites, dunites, pyroxenite, harzburgite, and lherzolite, and probably some amount of fluids from different origins, crustal and mantle which favor magmatic processes that accentuate the heterogeneous character of the mantle beneath the crustal root.

6. Conclusions

During the multiseismic URSEIS'95 experiment, a densely sampled wide-angle shot record was acquired using the normal incidence 18-km-long seismic reflection recording system. The shot gather, once reduced by 6 km/s, gives a high-resolution wide-angle seismic image of the upper mantle, and displays the crustal seismic phases within the first 2 s. A high amplitude PmP arrival can be identified. Reflected energy can be observed for up to 5 s twt beneath the PmP arrival. Beneath 5 s after the PmP event, the reflected energy decreases; however, a few events with some lateral correlation can be identified. Amplitude decay curves and frequency content support the argument that these reflections originated within the mantle. The character of the wide-angle shot gather suggests that the upper mantle is strongly heterogeneous beneath the Urals. It also suggests that at an approximate depth of 120–150 km the degree of heterogeneity decreases so that less seismic energy is reflected. The seismic image is consistent with an upper mantle consisting of two layers differentiated by their degree of heterogeneity; a shallower strongly heterogeneous layer and a deeper and more homogeneous one. If these layers are interpreted as the lithosphere and the asthenosphere, the wide-angle shot gather images the lithosphere–asthenosphere boundary. The lithosphere would be reflective while the asthenosphere would be less reflective. The estimated temperature depth diagram and "stratigraphy" derived from mantle xenoliths are consistent with the seismically proposed model. The 50-m trace spacing used in the acquisition of this

wide-angle shot gather resulted in one of the highest resolution wide-angle images of the subcrustal lithosphere beneath a root zone providing a new insight into processes that are not commonly imaged in seismic surveys of other orogenic zones, and therefore this data set should promote the design of high dense wide-angle seismic acquisition experiments.

Acknowledgements

Funding for this research was provided by the Ministerio de Ciencia y Tecnologia under grants: BTE2000-3035-E, REN2001-4230-E and by the Generalitat de Catalunya under Grant 2001SGR00339. This paper has benefited from the comments of A. Pérez-Estaún and F. Bea and from the helpful reviews by L. Nielsen, and an anonymous reviewer.

References

Anderson, D., 1990. Geophysics of the continental mantle: and historical perspective. In: Menzies, M. (Ed.), Continental Mantle, Oxford Monogr. Geol. Geophys. Oxford Sci. Publ., Oxford, pp. 1–3.

Berzin, R., Onken, O., Knapp, J., Pérez-Estaún, A., Hismatulin, T., Yunusov, N., Lipilin, A., 1996. Orogenic evolution of the Ural Mountains: results from a integrated seismic experiment. Science 274, 220–221.

Boyd, F., 1984. Siberian geotherm based on lherzolite xenoliths from Uldachnaya kimberlite, USSR. Geology 12, 528–530.

Calvert, A., Sawyer, E., Davis, W., J. Ludden, J., 1995. Archean subduction inferred from seismic images of mantle suture in the superior province. Nature 375, 670–674.

Carbonell, R., Gallart, J., Perez-Estaun, A., Diaz, J., Kashubin, S., Mechie, J., Wenzel, F., Knapp, J., 2000. Seismic wide-angle constraints on the crust of the Southern Urals. J. Geophys. Res. 105, 13755–13777.

Carbonell, R., Gallart, J., Perez-Estaun, A., 2002. Modelling and imaging the Moho transition: the case of the Southern Urals. Geophys. J. Int. 149, 134–148.

Carmichael, R., 1989. Physical Properties of Rocks and Minerals. CRC Press, Boston. 739 pp.

Chen, Y., O'Reilly, S., Kinny, P., Griffin, W., 1994. Dating lower crust and mantle events: and ion microprobe study of xenolith from kimberlitic pipes, South Australia. Lithos 32, 77–94.

Cook, F., Van der Velden, A., Hall, K.W., Roberts, B.J., 1999. Frozen subduction in Canada's north-western territories: lithoprobe deep lithospheric reflection profiling of the western Canadian shield. Tectonics 18, 1–24.

Downes, H., 1997. Shallow continental lithospheric mantle heterogeneity: petrological constraints. In: Fuchs, K. (Ed.), Upper Mantle Heterogeneities from Active and Passive Seismology. Kluwer Academic, Netherlands, pp. 295–308.

Echtler, H., Stiller, M., Steinhoff, F., Krawczyk, C., Suleimanov, A., Spiridonov, V., Knapp, J., Menshikov, Y., Alvarez-Marrón, J., Yunusiv, N., 1996. Preserved collisional crustal structure of the southern Urals revealed by Vibroseis profiling. Science 274, 224–226.

Gaherty, J.B., Jordan, T., 1995. Lehmann discontinuity as the base of an anisotropic layer beneath continents. Science 268, 1468–1471.

Gao, S., Kern, H., Liu, Y.S., Jin, S.Y., Popp, T., Jin, Z.M., Feng, J.I., Sun, M., Zhao, A.B., 2000. Measured and calculated seismic velocities and densities for granulites from xenolith occurrences and adjacent exposed lower crustal sections: a comparative study from the north China craton. J. Geophys. Res. 105, 18965–18976.

Griffin, W., Ryan, C., 1995. Trace elements in indicator minerals: area selection and target evaluation in diamond exploration. J. Geochem. Explor. 53, 311–337.

Griffin, W., Kaminsky, F., Ryan, C., O'Reilly, S., Win, T., Ilupin, I., 1996. Thermal state and composition of the lithospheric mantle beneath the Daldyn Kimberlite field, Yakutia. Tectonophysics 262, 19–33.

Guggisberg, B., Berthelesen, A., 1997. A two-dimensional velocity model for the lithosphere beneath the Baltic shield and its possible tectonic significance. Terra Cogn. 7, 631–638.

Hajnal, Z., Nemeth, B., Clowes, R.M., Ellis, R.M., Spence, G.D., Burianyk, M.J.A., Asudeh, I., White, D.J., Forsyth, D.A., 1997. Mantle involvement in the lithospheric collision: seismic evidence from Trans-Hudson orogen, Western Canada. Geophys. Res. Lett. 24, 2079–2082.

Henstock, T., Levander, A., and the Deep Probe Working Group, 1998. Probing the archean and proterozoic lithosphere of western North America. GSA Today 8 (1–5), 16–17.

Iyer, H., Hitchcock, H., 1989. Upper-mantle velocity structure in the continental U.S. and Canada. In: Pakiser, L., Mooney, W. (Eds.), Geophysical Framework of the Continental United States. Mem. Geol. Soc. Amer. 172, 681–710.

Jeffreys, H., 1936. The structure of the Earth down to the 20° discontinuity. Mon. Not. R. Astron. Soc. Geophys. Suppl. 3, 401–422.

Kern, H., Gau, S., Jin, Z., Popp, T., Jin, S., 1999. Petrophysical studies on rocks from the Dabie ultrahigh pressure (UHP) metamorphic belt, central China: implications for the composition of the lower crust. Tectonophysics 301, 191–215.

Lehmann, I., 1964. On the travel times of P as determined from nuclear explosions. Bull. Seismol. Soc. Am. 54, 123–129.

Levander, A., Holliger, K., 1992. Small-scale heterogeneity and large scale velocity structure of the continental crust. J. Geophys. Res. 97, 8797–8804.

Long, D., Christensen, N.I., 2000. Seismic anisotropy of South African upper mantle xenolith. Earth Planet. Sci. Lett. 179, 551–565.

Mechie, J., Yegorkin, A., Fuchs, K., Ryberg, T., Solodilov, L., Wenzel, F., 1993. P-wave mantle velocity structure beneath northern Eurasia from long-range recordings along the profile QUARTZ. Phys. Earth Planet. Inter. 79, 269–286.

Menke, W., Richards, P., 1983. Crust–mantle whispering gallery phase: a deterministic model of teleseismic Pn propagation. J. Geophys. Res. 85, 5416–5422.

Morgan, J.P., 1997. The generation of a compositional Lithosphere by mid-ocean ridge melting and its effect on subsequent off-axis hotspot upwelling and melting. Earth Planet. Sci. Lett. 146, 213–232.

Morgan, J.P., Morgan, W.J., 1999. Two-stage melting and geochemical evolution of the mantle: a recipe for mantle plum-pudding. Earth Planet. Sci. Lett. 170, 215–239.

Morozov, I.B., Smithson, S.B., 2002. Imaging crustal structure along refraction profiles using multicomponent recordings of first-arrival coda. BSSA 98 (8), 3080–3086.

Morozov, I.B., Morozova, E.A., Smithson, S.B., 1998. On the nature of the teleseismic Pn phase observed in the recordings from the ultra-long profile "Quartz", Russia. Bull. Seismol. Soc. Am. 88, 62–73.

Nielsen, L., Thybo, H., Morozov, I.B., Smithson, S.B., Solodilov, L., 2003a. Teleseismic Pn arrivals: influence of upper mantle velocity gradient and crustal scattering. Geophys. J. Int. 153, F1–F7.

Nielsen, L., Thybo, H., Levander, A., Solodilov, L., 2003b. Origin of upper mantle seismic scattering—evidence from Russian PNE data. Geophys. J. Int. 154, 196–204.

Nolet, G., 1994. Seismic heterogeneity in the upper mantle. J. Geophys. Res. 99, 23753–23766.

Pavlenkova, N.I., 1996. General features of the uppermost mantle stratification from long-range seismic profiles. Tectonophysics 264, 261–278.

Perchuc, E., Thybo, H., 1996. A new model of upper mantle P-wave velocity below the Baltic shield: indication of partial melt in the 95 to 160 km depth range. Tectonophysics 253, 227–245.

Priestley, K., 1999. Velocity structure of the continental upper mantle: evidence from Southern Africa. Developments in Geotectonics. Elsevier, Amsterdam, pp. 45–46.

Posgay, K., Hegedus, E., Timar, Z., 1990. The identification of mantle reflections below Hungary from deep seismic profiling. Tectonophysics 173, 379–385.

Ryan, C., Griffin, W., Pearson, N., 1996. Garnet geotherms: derivation of *P–T* data from chrome-pyrope garnets. J. Geophys. Res. 101, 5611–5625.

Ryberg, T., Wenzel, F., 1999. High-frequency wave propagation in the uppermost mantle. J. Geophys. Res. 104, 10.655–10.666.

Ryberg, T., Fuchs, K., Yegorkin, A., Solodilov, L., 1995. High-frequency teleseismic Pn wave observations beneath northern Eurasia. J. Geophys. Res. 100, 18151–18163.

Ryberg, T., Tittgemeyer, M., Wenzel, F., 2000. Finite difference modelling of P-wave scattering in the upper mantle. Geophys. J. Int. 141, 787–800.

Steer, D., Knapp, J., Brown, L., 1998. Super-deep reflection profiling: exploring the continental mantle lid. Tectonophysics 286, 111–121.

Thybo, H., Perchuc, E., 1997. The seismic 8° discontinuity and partial melting in the continental mantle. Science 275, 1626–1629.

Tittgemeyer, M., Wenzel, F., Fuchs, K., Ryberg, T., 1996. Wave propagation in a multiple scattering upper-mantle: observations and modelling. Geophys. J. Int. 127, 492–502.

Tittgemeyer, M., Wenzel, F., Ryberg, T., Fuchs, K., 1999. Scales of heterogeneities in the continental crust and upper mantle. Pure Appl. Geophys. 156, 29–52.

Warner, W., Morgan, J., Barton, P., Morgan, P., Price, C., Jones, K., 1996. Seismic reflections from the mantle represent relict subduction zones within the continental lithosphere. Geology 24, 39–42.

Willmore, P.L., 1949. Seismic experiments on the North German explosions 1946 to 1947. Philos. Trans. R. Soc. Lond., A 242, 123–151.

Yegorkin, A., Zuganov, S., Pavlenkova, N., Chernyshev, N.N., 1987. Results of lithosphere studies from long-range profiles in Siberia. Tectonophysics 140, 29–47.

Zhao, J., McCulloch, M., 1993. Melting of a subduction-modified continental lithospheric mantle; evidence from late proterozoic mafic dyke swarms in central Australia. Geology 21, 463–466.